Acta Mech 233, 1467–1483 (2022)
https://doi.org/10.1007/s00707-022-03177-8

ORIGINAL PAPER

Mohsen Gorakifard · Clara Salueña · Ildefonso Cuesta · Ehsan Kian Far

The meshless local Petrov–Galerkin cumulant lattice Boltzmann method: strengths and weaknesses in aeroacoustic analysis

Received: 10 August 2021 / Revised: 30 January 2022 / Accepted: 25 February 2022 / Published online: 6 April 2022

Abstract The lattice Boltzmann method (LBM) suffers from an instability at low viscosities and from having to compromise between accuracy and computational efficiency due to its lattice uniformity. Thus, in this paper, the meshless local Petrov–Galerkin cumulant lattice Boltzmann method (MLPGC-LBM) is proposed to remedy these shortcomings. The collision step is modeled by the cumulant method, stable at low viscosities, and the streaming step is discretized first in time based on the Lax–Wendroff scheme, then in space according to the meshless local Petrov–Galerkin method, a mesh-free method (MLPG). To substantiate the accuracy of this method in aeroacoustics, the temporal decay of a standing plane wave, the spatial decay of a planar acoustic pulse, and the propagation of circular waves are considered, and the results are compared with numerical and analytical solutions. The comparisons show that MLPGC-LBM presents better results than standard LB methods, replicating the local radial point interpolation cumulant lattice Boltzmann method (LRPIC-LBM) results with relatively shorter runtimes, and being in a good agreement with the analytical solutions. The errors of the acoustic dispersion and dissipation are irrelevant, even for quite low resolutions. Therefore, MLPGC-LBM can offer an alternative to conventional aeroacoustics simulations alongside LRPIC-LBM with shorter runtimes, without parametric dependency on the number of points per wavelength and the resolution

1 Introduction

The lattice Boltzmann method (LBM), an explicit time marching scheme [1], has recently been used in many different fields of fluid mechanics. Originated from the lattice gas automata, the LBM simplifies the implementation and facilitates the parallelization of simulations of engineering problems with complex geometries. It dramatically saves time and efforts using probability density functions (probability of detecting particles in a specific range of velocities and locations at a given time), to determine the momentum distribution in discrete space [2]. However, the LBM is restricted by the lattice uniformity resulting from the symmetries of the lattice velocity model assumed. Such limitation causes the LBM suffer from accuracy and efficiency issues in simulations needing non-uniform meshes [3] such as those with irregular boundaries. Even though schemes using grid refinement improve accuracy substantially [4], they also pose new challenges like higher computational cost and even the appearance of additional perturbations in acoustical problems [5].

Conventional non-uniform LB methods have been categorized in different types: interpolation-supplemented LBM [6,7], combinations of LBM with finite difference methods [8], finite volume methods [9–11], finite element methods [12–14], and Taylor-series expansion and least-squares-based lattice Boltzmann

M. Gorakifard (✉) · C. Salueña · I. Cuesta
Department of Mechanical Engineering, ETSEQ, Rovira i Virgili University, Països Catalans, 26, 43007 Tarragona, Spain
E-mail: mohsen.goraki@urv.cat

E. K. Far
Siemens Digital Industries Software, Nottingham, UK

methods [15,16]. These methods have succeeded in simulating different problems; however, they suffer from drawbacks such as mesh generating costs, low accuracy of the computed stress in fluid-structure interaction simulations [17], and a disability to model singular physical phenomena. Thus, mesh-free methods are devised to deal with such obstacles [18,19] by using a set of nodes called field nodes, scattered inside and on the boundaries of the domain. These methods generate a system of algebraic equations for the field nodes, without the need to explicitly link them in order to interpolate or approximate the unknown variables.

MFree methods have been developed along with old methods like the collocation method [20,21], vortex method [22], finite difference method [23–25], and smoothed particle hydrodynamics [26,27]. Among the MFree methods classified according to their formulation procedure, the so called weak-form methods have attracted the interest of many researchers and are broadly expanded [18], such as the diffuse element method [28], the local radial point interpolation method (LRPIM) [29], the local point interpolation method (LPIM) [30], and the meshless local Petrov–Galerkin method (MLPG) [31]. The idea of combining LBM and Mfree methods has led to acceptable results in some cases [32–34]. These studies use the standard Bhatnagar–Gross–Krook (BGK) approach which is not stable at high Reynolds numbers and low viscosities [35,36]. Thus, combining the more stable cumulant LBM [37,38] with Mfree-LB methods could provide better results in different engineering problems. This is the case when using the local radial point interpolation cumulant lattice Boltzmann method (LRPIC-LBM) [39]. It can predict analytical results without parameter dependencies such as the number of points per wavelength N_{ppw}, and the resolution σ. In addition, as it will be shown in the following, the efficiency of Mfree-LB methods could be increased by substituting the local radial point interpolation method with the meshless local Petrov–Galerkin method in the Mfree part, due to the fact that radial point interpolation method shape functions used in LRPIM need more computational resources than moving least squares (MLS) shape functions used in MLPG.

The main objective of this paper is to study the ability of the meshless local Petrov–Galerkin cumulant LBM (MLPG-LBM) to simulate aeroacoustics problems and compute the errors and deviations from the experimental and standard LBM, and LRPIC-LBM results. Thus, the LB equation is split into the collision part, modeled by the cumulant method, and the streaming part which is discretized first in time using the Lax–Wendroff scheme, then in space utilizing MLPG. This plan is developed in the following Sections. Firstly, a brief explanation of our new LB method is presented in Sect. 2. The LBM steps (the collision step and the streaming step) are discussed in Sects. 2.1 and 2.2. The crucial details of the Mfree shape function construction, time discretization (Lax–Wendroff scheme), and space discretization (MLPG) are explained in Sects. 2.2.1, 2.2.2, and 2.2.3. The results of the MLPG-LBM simulations of the propagation of a planar standing wave, a planar pulse wave, an acoustic 2D pulse, and an acoustic point source are reported and discussed in Sect. 3.

2 Lattice Boltzmann method

The lattice Boltzmann method (LBM), derived from the kinetic theory of gases, has been a good substitute for solving the Navier–Stokes equations to model different fluid flow phenomena. In this method, a set of probability density functions [3] plays a key role in modeling the momentum distribution in discrete space. The standard force-free lattice Boltzmann equation is

$$f_i\left(x_\alpha + c_{i,\alpha}\Delta t, t + \Delta t\right) - f_i\left(x_\alpha, t\right) = \Omega_i \tag{1}$$

where x and c_i are the particle position and lattice speed, f_i is the particle distribution function, and Ω_i is the collision operator. For a 2D problem, x_α is equal to $[x, y]$.

The LBM is divided into collision and streaming steps. The cumulant method for the collision part, and the meshless local Petrov–Galerkin method (MLPG) for the streaming part, are adopted to introduce the meshless local Petrov–Galerkin cumulant lattice Boltzmann method (MLPG-CLBM) as follows.

2.1 Collision step

The cumulant LBM was proposed by Seeger to solve the Boltzmann equation [40,41]. It can improve the cascade LBM [42,43] developed to ease instability issues of previous models, by removing the lower-order moment effects on the higher-order moments using a transformation to a set of functions. The central moments can efficiently give the cumulants of a distribution function. The cumulant LBM can be briefly explained as follows.

Considering the local momentum distribution function, f_i as a probability mass function consisting of two random variables ξ, υ with ranges $R_\xi = \{\xi_1, \xi_2, \ldots\}$, $R_\upsilon = \{\upsilon_1, \upsilon_2, \ldots\}$ based on the microscopic velocities in x, y directions, the probability density function [3] is

$$\boldsymbol{f}(\xi, \upsilon) = \sum_{ij} f(\xi_i, \upsilon_j)\delta(\xi - \xi_i)\delta(\upsilon - \upsilon_i). \tag{2}$$

To obtain moments without discontinuity issues, the moment generating function, $M(\Xi, \Upsilon) = \sum_{ij} f(\xi_i, \upsilon_j)e^{\Xi\xi_i}e^{\Upsilon\upsilon_j}$, is used, where Ξ and Υ are the normalized wave numbers [44],

$$\mu'_{\xi^m\upsilon^n} = \frac{\partial^m\partial^n}{\partial\Xi^m\partial\Upsilon^n}M(\Xi, \Upsilon)|_{\Xi=\Upsilon=0}, \tag{3}$$

To reduce Galilean relativity issues in the collision scheme, the moment generating function can be shifted to the reference frame of the moving fluid. Thus, the central moments can be obtained by [45]

$$\mu_{\xi^m\upsilon^n} = \frac{\partial^m\partial^n}{\partial\Xi^m\partial\Upsilon^n}\widehat{M}(\Xi, \Upsilon)|_{\Xi=\Upsilon=0} \tag{4}$$

where $\widehat{M}(\Xi, \Upsilon) = e^{-\Xi u/c - \Upsilon v/c}M(\Xi, \Upsilon)$ is the central moment generating function.

The cumulants are calculated as follows [46]:

$$c_{\xi^m\upsilon^n} = \frac{\partial^m\partial^n}{\partial\Xi^m\partial\Upsilon^n}\ln(M(\Xi, \Upsilon))|_{\Xi=\Upsilon=0}. \tag{5}$$

It should be mentioned that cumulants relax with individual relaxation rates,

$$c^*_{\xi^m\upsilon^n} = c_{\xi^m\upsilon^n} + \omega_{\xi^m\upsilon^n}(c^{eq}_{\xi^m\upsilon^n} - c_{\xi^m\upsilon^n}), \tag{6}$$

where $c^{eq}_{\xi^m\upsilon^n}$ are the equilibrium state cumulants.

The LBM is not completely incompressible but has a finite bulk viscosity as a function of the relaxation rate. This bulk viscosity damps down pressure waves: the higher the values of the bulk viscosity the faster the decay of pressure waves in the system. The BGK model, with a single relaxation rate, is only stable at low enough Reynolds numbers, but at higher Re the bulk viscosity does not reduce the effects of pressure waves, and the method becomes unstable. This problem is fixed by using a LBM model with different relaxation rates. Thus, the main goal of developing such models was to maximize the number of adjustable parameters to improve both stability and accuracy. These methods employ a transformation into equivalent different spaces –such as the cumulant space, which associates physical quantities with the cumulants of the distribution functions. In these models, some relaxation parameters are chosen to satisfy the physical parameters of the fluid, whereas the rest are selected to render the method more stable. Therefore, the second group of parameters can increase or decrease the stability of the method depending on their values. In addition, the violation of Galilean invariance affecting the BKG model is not observed in the cumulant model under the same conditions [3]. Similarly, relaxation rates for the second cumulants are calculated with the shear viscosity, and as for the rest of relaxation rates (for the third and fourth cumulants), the value of 1 is selected to minimize instabilities. The sound speed and the shear viscosity are determined as $c_s = \Delta x/(\sqrt{3}\Delta t)$ and $\nu = \Delta t^2(1/\omega - 0.5)$ [47], respectively.

The kernel algorithm to implement the cumulant LBM can be summarized in the following steps [48]; Step 1: Calculating the central moments of the distribution function using Eq. (4), Step 2: Determining cumulants using the central moments, Step 3: Acquiring post-collision cumulants from the collision operator based on Eq. (6). Step 4: Extracting post-collision central moments from the post-collision cumulants, Step 5: Transferring the post-collision central moments back to the distribution functions [3].

2.2 Streaming step

The second key element of LBM is the streaming process. Generally, this step is implemented by solving a pure advection equation from a Lagrangian point of view within uniform structured meshes. Therefore, the CFL number is considered to be unity. By changing the perspective to an Eulerian point of view, it is possible to deal with such limitation. The pure advection equation is

$$\frac{\partial f_i}{\partial t} + c_{i,\alpha}\frac{\partial f_i}{\partial x_\alpha} = 0. \tag{7}$$

Equation (7), a time-dependent equation, is discretized based on a semi-discrete formulation. Thus, the Lax–Wendroff scheme and meshless local Petrov–Galerkin method (MLPG) are separately used for time and space discretization. Moreover, the unknown field function f_i can be estimated by trial (shape) functions as an approximate solution for the PDE. In this paper, moving least squares shape functions are chosen.

2.2.1 Mfree shape function construction—moving least squares shape functions

The moving least squares (MLS) approximation developed by mathematicians in the field of data fitting [49] has been used for constructing MFree shape functions. It is classified as a method of series approximation of functions.

In the MLS approximation, the distribution function is approximated by $f^h(x_\alpha, t)$ as

$$f(x_\alpha, t) \approx f^h(x_\alpha, t) = \sum_{i=1}^{m} p_i(x_\alpha) a_i(x_\alpha, t) = \boldsymbol{p}^T(x_\alpha)\boldsymbol{a}(x_\alpha, t) \tag{8}$$

where m, $p_i(x_\alpha)$, and $a_i(x_\alpha, t)$ are the number of basis functions, the basis functions, and their corresponding coefficients, respectively. The coefficient $\boldsymbol{a}$ is determined by minimizing the difference between the local approximation and the function according to the formula

$$J = \sum_{i=1}^{n} w_i(x_\alpha)\left[\boldsymbol{p}^T(x_{i,\alpha})\boldsymbol{a}(x_\alpha, t) - f_i(t)\right]^2, \tag{9}$$

where n is the number of nodes in the support domain of x_α for the weight function $w_i(x_\alpha) = w(x_\alpha - x_{i,\alpha}) \neq 0$ with a compact support associated with node $x_{i,\alpha}$ and maximum at node $x_{i,\alpha}$. In addition, $f_i(t) = f(x_{i,\alpha}, t)$ is the nodal value of the function $f(x_\alpha, t)$. It is called nodal parameter given that $f_i(t) \neq f^h(x_{i,\alpha}, t)$ in the MLS approximation.

Minimizing the functional J leads to

$$\boldsymbol{A}(x_\alpha)\boldsymbol{a}(x_\alpha, t) = \boldsymbol{B}(x_\alpha)\boldsymbol{F}(t), \tag{10}$$

where

$$\boldsymbol{A}(x_\alpha) = \sum_{i=1}^{n} w_i \boldsymbol{p}(x_{i,\alpha})\boldsymbol{p}^T(x_{i,\alpha}) = \begin{bmatrix} \sum_{i=1}^{n} w_i & \sum_{i=1}^{n} x_i w_i & \sum_{i=1}^{n} y_i w_i \\ \sum_{i=1}^{n} x_i w_i & \sum_{i=1}^{n} x_i^2 w_i & \sum_{i=1}^{n} x_i y_i w_i \\ \sum_{i=1}^{n} y_i w_i & \sum_{i=1}^{n} x_i y_i w_i & \sum_{i=1}^{n} y_i^2 w_i \end{bmatrix}, \tag{11}$$

$$\begin{aligned} \boldsymbol{B}(x_\alpha) &= \left[w_1(x_\alpha)\boldsymbol{p}(x_{1,\alpha}), w_2(x_\alpha)\boldsymbol{p}(x_{2,\alpha}), \ldots, w_n(x_\alpha)\boldsymbol{p}(x_{n,\alpha})\right] \\ &= \begin{bmatrix} w_1 & w_2 & \ldots & w_n \\ x_1 w_1 & x_2 w_2 & \ldots & x_n w_n \\ y_1 w_1 & y_2 w_2 & \ldots & y_n w_n \end{bmatrix}, \end{aligned} \tag{12}$$

$$\boldsymbol{F}(t) = [f_1(t), f_2(t), \ldots, f_n(t)]^T. \tag{13}$$

Estimating $\boldsymbol{a}(x_\alpha, t)$ from Eq. (10), and substituting it into Eq. (8), results in the following final form:

$$f^h(x_\alpha, t) = \sum_{i=1}^{n} \phi_i(x_\alpha) f_i(t) = \boldsymbol{\Phi}(x_\alpha) \boldsymbol{F}(t), \tag{14}$$

where

$$\boldsymbol{\Phi}^T(x_\alpha) = \{\phi_1(x_\alpha) \quad \phi_2(x_\alpha) \quad \dots \quad \phi_n(x_\alpha)\} = \boldsymbol{p}^T(x_\alpha) \boldsymbol{A}^{-1}(x_\alpha) \boldsymbol{B}(x_\alpha), \tag{15}$$

and the shape function ϕ_i for the i-th node is $\phi_i(x_\alpha) = \boldsymbol{p}^T(x_\alpha) \left(\boldsymbol{A}^{-1}\boldsymbol{B}\right)_i$.

Unlike the finite-element approximation, the continuity of the moving least squares approximation depends not only on the basis functions, but also on the weight functions. Having C^l and C^k as the continuity classes for the basis functions and the weight functions, respectively, results in $C^{\min(l,k)}$ for the continuity of the moving least squares shape function. Since the base functions are infinitely differentiable monomial functions, the properties of the weight functions become thus determinant. Among the different types of weight functions employed in meshless methods, the cubic spline function is used in this paper,

$$V_i(r) = \begin{cases} \frac{2}{3} - 4r^2 + 4r^3 & r \le 0.5 \\ \frac{4}{3} - 4r + 4r^2 - \frac{4}{3}r^3 & 0.5 < r \le 1, \\ 0 & r > 1 \end{cases} \tag{16}$$

where $r = \left|x_\alpha - x_{i,\alpha}\right| / d^{\max}$, and $d^{\max}$ is the radius of the compact support.

2.2.2 Semi-discrete formulation—time discretization

Using the Taylor series expansion of the particle distributions and substituting the time derivatives with the spatial derivatives up to second order, the time discretization of equation (7) according to the Lax–Wendroff scheme is obtained as

$$f_i^{n+1} = f_i^n - \Delta t c_{i,\alpha} \frac{\partial f_i^n}{\partial x_\alpha} + \frac{\Delta t^2}{2} c_{i,\alpha} c_{i,\beta} \frac{\partial^2 f_i^n}{\partial x_\alpha \partial x_\beta} \tag{17}$$

where here n refers to the time step.

2.2.3 Semi-discrete formulation—space discretization

The meshless local Petrov–Galerkin (MLPG) method, a local weak-form, is proposed to avoid global background cells for either function approximation or integration. The numerical integrations are executed over a local quadrature domain consisting of a set of distributed nodes. It should be mentioned that the MLS approximation is utilized to construct the shape functions in MLPG, which results in improving the efficiency of the scheme beyond that of the LRPM.

Generally, the weak form of the problem generated from the method of weighted residuals is used for MFree local weak-form methods. Thus, the weighted residual form of Eq. (17) on the local domain Ω_I of point I bounded by Γ_I is

$$\int_{\Omega_I} V_I f_i^{n+1} \, \mathrm{d}\Omega = \int_{\Omega_I} V_I f_i^n \, \mathrm{d}\Omega - \Delta t \int_{\Omega_I} V_I c_{i,\alpha} \frac{\partial f_i^n}{\partial x_\alpha} \, \mathrm{d}\Omega + \frac{\Delta t^2}{2} \int_{\Omega_I} V_I c_{i,\alpha} c_{i,\beta} \frac{\partial^2 f_i^n}{\partial x_\alpha \partial x_\beta} \, \mathrm{d}\Omega \tag{18}$$

where V_I is the local weight function of node I introduced in Eq. (16). Equation (18) is employed for all nodes in the domain.

Using integration by parts in Eq. (18), a continuous approximate solution is obtained, and the differentiation requirements of the unknowns in the weighted residual form are reduced,

$$\begin{aligned} \int_{\Omega_I} V_I f_i^{n+1} \, \mathrm{d}\Omega = \int_{\Omega_I} V_I f_i^n \, \mathrm{d}\Omega - \int_{\Omega_I} \left(\Delta t V_I c_{i,\alpha} \frac{\partial f_i^n}{\partial x_\alpha} + \frac{\Delta t^2}{2} c_{i,\alpha} c_{i,\beta} \frac{\partial V_I}{\partial x_\beta} \frac{\partial f_i^n}{\partial x_\alpha} \right) \mathrm{d}\Omega \\ + \frac{\Delta t^2}{2} \int_{\Gamma_I} V_I c_{i,\alpha} c_{i,\beta} \frac{\partial f_i^n}{\partial x_\alpha} n_\beta \, \mathrm{d}\Gamma, \end{aligned} \tag{19}$$

where Γ_I and n_β are, respectively, the boundary of the local domain Ω_I and the unit outward normal vector.

Substitution of the approximate solution (14) into Eq. (19) gives

$$\sum_{J=1}^{N_I} M_{IJ} f_{i,J}^{n+1} = \sum_{J=1}^{N_I} \left[M_{IJ} + K_{i,IJ} \right] f_{i,J}^{n} \tag{20}$$

where M_{IJ} is the nodal mass matrix and $K_{i,IJ}$ is the nodal stiffness matrix, written as

$$M_{IJ} = \int_{\Omega_I} V_I \phi_J \, \mathrm{d}\Omega, \tag{21}$$

$$K_{i,IJ} = -\int_{\Omega_I} \left(\Delta t V_I + \frac{\Delta t^2}{2} c_{i,\beta} \frac{\partial V_I}{\partial x_\beta} \right) c_{i,\alpha} \frac{\partial \phi_J}{\partial x_\alpha} \, \mathrm{d}\Omega + \frac{\Delta t^2}{2} \int_{\Gamma_I} V_I c_{i,\alpha} \frac{\partial \phi_J}{\partial x_\alpha} c_{i,\beta} n_\beta \, \mathrm{d}\Gamma. \tag{22}$$

Therefore, the global equation system for all nodes in the whole domain is expressed by

$$\boldsymbol{M} \boldsymbol{f}_i^{n+1} = [\boldsymbol{M} + \boldsymbol{K}_i] \, \boldsymbol{f}_i^{n} \tag{23}$$

where $\boldsymbol{f}_i$, $\boldsymbol{M}$, and $\boldsymbol{K}$ are the particle distribution vector, the global mass matrix, and stiffness matrix, respectively. This system is worked out separately for each direction.

Using the Gauss quadrature scheme leads to the numerical area and curve integration of Eqs. (21) and (22),

$$M_{IJ} = \sum_{\kappa=1}^{n_g} \widetilde{\zeta}_\kappa V_I \left(x_\kappa \right) \phi_J \left(x_\kappa \right) \left| J^{\Omega_I} \right|, \tag{24}$$

$$\begin{aligned} K_{i,IJ} = & -\sum_{\kappa=1}^{n_g} \widetilde{\zeta}_\kappa \left(\Delta t V_I(x_\kappa) + \frac{\Delta t^2}{2} c_{i,\beta} \left. \frac{\partial V_I}{\partial x_\beta} \right|_{x_\kappa} \right) c_{i,\alpha} \left. \frac{\partial \phi_J}{\partial x_\alpha} \right|_{x_\kappa} \left| J^{\Omega_I} \right| \\ & + \frac{\Delta t^2}{2} \sum_{\kappa=1}^{n_g^b} \widetilde{\zeta}_\kappa V_I(x_\kappa) c_{i,\alpha} \left. \frac{\partial \phi_J}{\partial x_\alpha} \right|_{x_\kappa} c_{i,\beta} n_\beta \left| J^{\Gamma_I} \right| \end{aligned} \tag{25}$$

where n_g, n_g^b, $\widetilde{\zeta}_\kappa$, J^{Ω_I}, and J^{Γ_I} are, respectively, the total number of Gauss points in the quadrature domain, the total number of Gauss points at the boundaries, the Gauss weight factor for Gauss point x_κ, the Jacobian matrix for the domain integrations, and the Jacobian matrix for boundary integrations.

3 Results and discussion

For direct simulations with reduction of computational costs, aeroacoustics has lately adopted the LBM. In this Section, the standard analysis consisting of obtaining acoustic properties for benchmark cases is studied using the meshless local Petrov–Galerkin cumulant lattice Boltzmann method (MLPGC-LBM). Here, the propagation of planar acoustic waves is considered, focusing on numerical dissipation and dispersion. In addition, circular wave propagations are studied. Expressing the total pressure as the sum of the atmospheric pressure p_0 and the acoustic pressure p', a lossy wave equation can be written [50] for p',

$$\left(c_s^2 + \left[\frac{4}{3} \nu + \nu_B \right] \frac{\partial}{\partial t} \right) \nabla^2 p' = \frac{\partial^2 p'}{\partial t^2}; \tag{26}$$

here ν and ν_B are the coefficients of shear and bulk viscosity, respectively. To have a better assessment of MLPGC-LBM, four setups based on [5,39] are examined including the temporal decay of a standing plane wave in a periodic domain, the spatial decay of a propagating planar acoustic pulse of Gaussian shape, a 2D acoustic pulse with Gaussian shape, and an acoustic point source for regular (default) and irregular nodal distributions (shown in Fig. 1a, b). The base units are in the LB system.

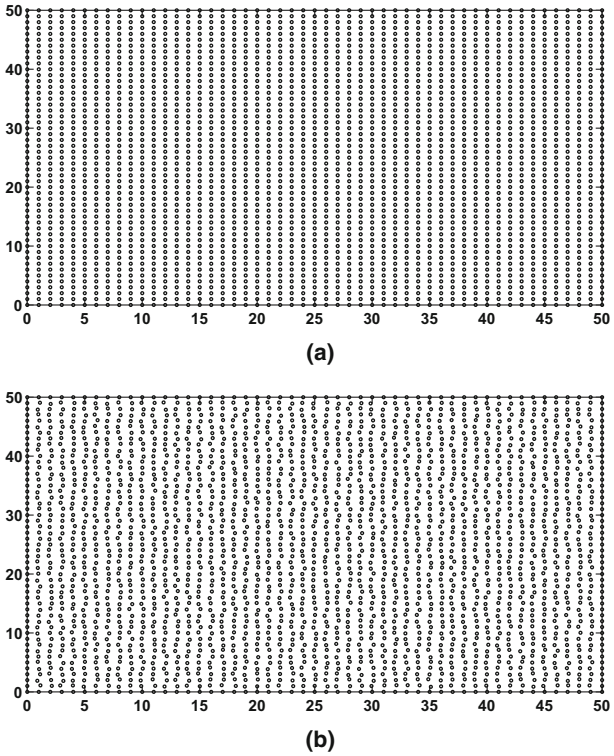

Fig. 1 Nodal arrangement for the propagation of planar acoustic waves in MLPGC-LBM simulations: **a** Regular nodes. **b** Irregular nodes

Table 1 Parameters for the planar standing wave

Variables	$p'(x, y, 0)$	ρ'	u'	v'	A
Description	$A \sin\left(\frac{2\pi x}{\lambda}\right)$	$\frac{p'}{c_s^2}$	$\frac{p'}{\rho_0 c_s}$	0	$10^{-3} p_0$

3.1 Planar standing wave

As a first configuration, a standing plane acoustic wave in a periodic domain is studied. The dissipation and dispersion relations obtained from Eq. (26) according to a temporal analysis are [51]

$$c_T = c_s \sqrt{1 - \left(\frac{k\nu}{c_s}\right)^2}, \tag{27.1}$$

$$\alpha_T = k^2 \nu \tag{27.2}$$

where k is the wave number. The assumptions for this setup are given as a reference in Table 1 [5,39] (where "$\prime$" is the perturbation quantity). The results of such study can be expressed either as a function of the number of points per wavelength $N_{\text{ppw}} = \lambda/\Delta x$, or the non-dimensional wave number $k\Delta x = 2\pi/N_{\text{ppw}}$.

The acoustic pressure at time t is [5,39]

$$p'(x, y, t) = A \exp\left[-\alpha_T t\right] \sin\left[k\,(x - c_T t)\right]. \tag{28}$$

To study the pros and cons of the meshless local Petrov–Galerkin cumulant lattice Boltzmann method (MLPGC-LBM), the propagation of waves with various viscosities, ν, and different resolutions (i.e. the number of points per wavelength) was investigated. The acoustic pressure time history for $\nu = 1.0 \times 10^{-2}$ $[\frac{\Delta x^2}{\Delta t}]$ with $N_{\text{ppw}} = 14$ points per wavelength is presented in Fig. 2. The analytical result is drawn with a solid black line while MLPGC-LBM with linear basis functions ($m = 3$) and quadric basis functions ($m = 6$) are shown with

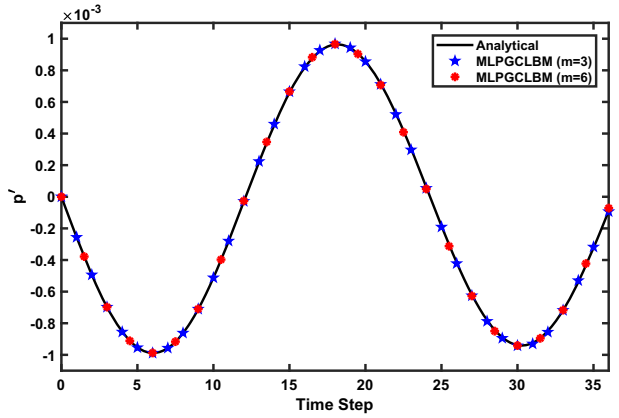

Fig. 2 Acoustic pressure $[\frac{kg}{\Delta x \Delta t^2}]$ versus time step $[\Delta t]$ for $\nu = 1.0 \times 10^{-2}$ $[\frac{\Delta x^2}{\Delta t}]$ with $N_{\text{ppw}} = 14$ points per wavelength

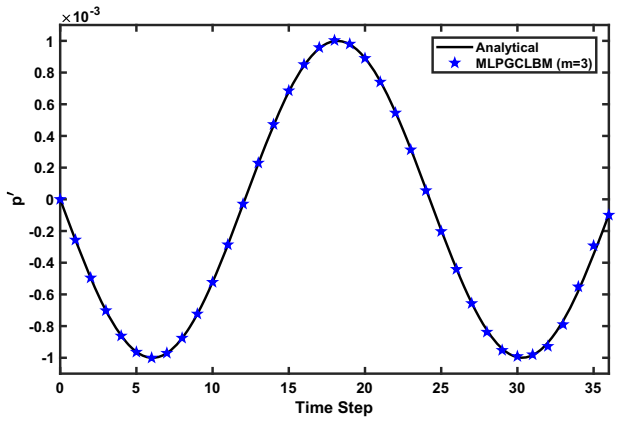

Fig. 3 Acoustic pressure $[\frac{kg}{\Delta x \Delta t^2}]$ versus time step $[\Delta t]$ for $\nu = 1.0 \times 10^{-4}$ $[\frac{\Delta x^2}{\Delta t}]$ with $N_{\text{ppw}} = 14$ points per wavelength

a blue five-pointed star and a red asterisk, respectively. It is shown that this method with linear and quadric basis functions gives a good prediction of the analytical acoustic pressure values.

Figure 3 shows the acoustic pressure time history for $\nu = 1.0 \times 10^{-4}$ $[\frac{\Delta x^2}{\Delta t}]$ with $N_{\text{ppw}} = 14$ points per wavelength. It draws a comparison between the analytical solution and the meshless local Petrov–Galerkin cumulant lattice Boltzmann method results with linear basis functions ($m = 3$) at low viscosities. One major drawback of standard LB methods is the instability that develops at low viscosities; however, this method even with linear basis functions shows a good performance and closely predicts the theoretical solution with negligible phase speed and temporal dissipation rate errors.

The numerical deviations of the acoustical properties for current standard LB methods are functions of N_{ppw} and are independent of other parameters such as the frequency and the viscosity. For example, the errors of the BGK [51] and the cumulant LBM [5] are about 7 percent for $N_{\text{ppw}} = 4$ for such properties. However, the advent of combined Mfree-LB methods such as the local radial point interpolation cumulant lattice Boltzmann method (LRPIC-LBM) makes it possible to predict wave motion with no dependency on the number of points per wavelength N_{ppw}. Figure 4 shows the acoustic pressure time history for $\nu = 1.0 \times 10^{-2}$ $[\frac{\Delta x^2}{\Delta t}]$ with $N_{\text{ppw}} = 4$ points per wavelength for the analytical solution (a solid black line), the cumulant LBM (a dashed red line), and the meshless local Petrov–Galerkin cumulant lattice Boltzmann method (MLPGC-LBM) with linear basis functions (magenta asterisk), with $\Delta t = 0.1$. It shows that MLPGC-LBM with linear basis functions is more successful in predicting theoretical results than the cumulant LBM, at a low number of points per wavelength.

In general, one of the characteristics of MLPGM is that the Kronecker delta condition is not satisfied, so the accuracy of the results obtained in the nodes is reduced. Among the ways presented in Ref. [18] to improve accuracy, we are interested in increasing the polynomial degree of the basis functions. Thus, by replacing the

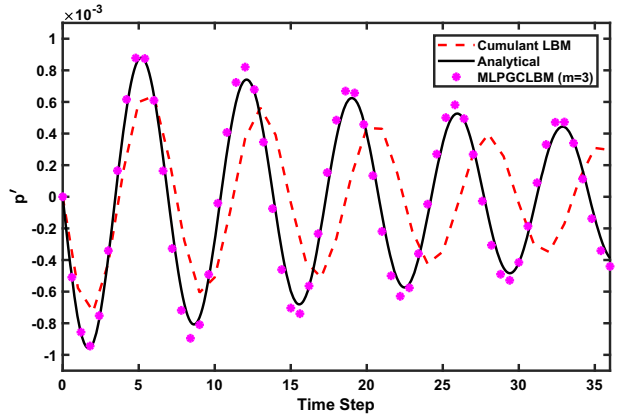

Fig. 4 Acoustic pressure $[\frac{kg}{\Delta x \Delta t^2}]$ versus time step $[\Delta t]$ for $\nu = 1.0 \times 10^{-2}$ $[\frac{\Delta x^2}{\Delta t}]$ with $N_{\text{ppw}} = 4$ points per wavelength and $\Delta t = 0.1$

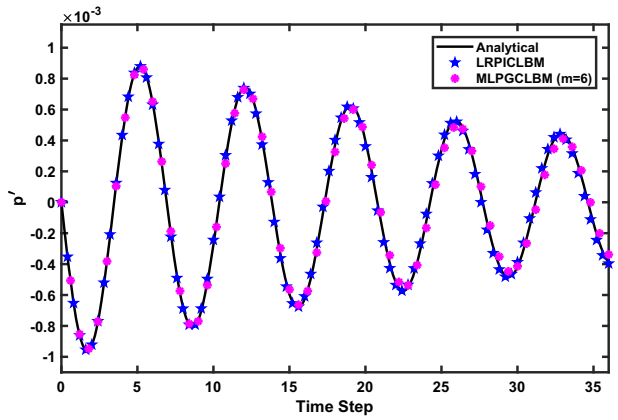

Fig. 5 Acoustic pressure $[\frac{kg}{\Delta x \Delta t^2}]$ versus time step $[\Delta t]$ for $\nu = 1.0 \times 10^{-2}$ $[\frac{\Delta x^2}{\Delta t}]$ with $N_{\text{ppw}} = 4$ points per wavelength with $\Delta t = 0.1$

linear basis functions with quadric ones in the meshless local Petrov–Galerkin cumulant lattice Boltzmann method (MLPGC-LBM), an improvement is achieved as we will show. Figure 5 shows the acoustic pressure time history for $\nu = 1.0 \times 10^{-2}$ $[\frac{\Delta x^2}{\Delta t}]$ with $N_{\text{ppw}} = 4$ points per wavelength for the analytical solution (black solid line), the local radial point interpolation cumulant lattice Boltzmann method (LRPIC-LBM) (blue five-point star), and the meshless local Petrov–Galerkin cumulant lattice Boltzmann method (MLPGC-LBM) solution with quadric basis functions ($m = 6$) (magenta asterisk), for $\Delta t = 0.1$. This Figure shows that both MLPGC-LBM and LRPIC-LBM replicate the analytical results. On the other hand, one of the pros of MLPGM is that its efficiency is higher than that of LRPIM due to the difference in the interpolation procedures (the moving least squares (MLS) shape functions). Therefore, MLPGC-LBM benefits from this feature. Moreover, for the acoustic pressure time history shown in Fig. 5, the average run time for the MLPGC-LBM is 0.285 times that of the LRPIC-LBM. Both methods give similar results, predicting wave motion accurately with no dependency on the number of points per wavelength N_{ppw}, but MLPGC-LBM needs lesser run times.

In many engineering problems such as those of acoustics, it is necessary to use irregular nodes. We have seen how MLPGC-LBM performs efficiently when it comes to predict the propagation of acoustic waves through domains with regular nodal distributions. However, the accuracy of this method should also be examined with irregular nodes (Fig. 1b). Figure 6 presents the acoustic pressure time history for $\nu = 1.0 \times 10^{-2}$ $[\frac{\Delta x^2}{\Delta t}]$ with $N_{\text{ppw}} = 14$ points per wavelength. It shows the comparison between analytical (solid black line) and MLPGC-LBM results determined with linear basis functions ($m = 3$) (blue five-pointed star) and quadric basis functions ($m = 6$) (red asterisk). It is shown that MLPGC-LBM with linear basis functions cannot reliably predict the motion of waves, and results soon depart from the theoretical solution. This issue is related to the lack of a

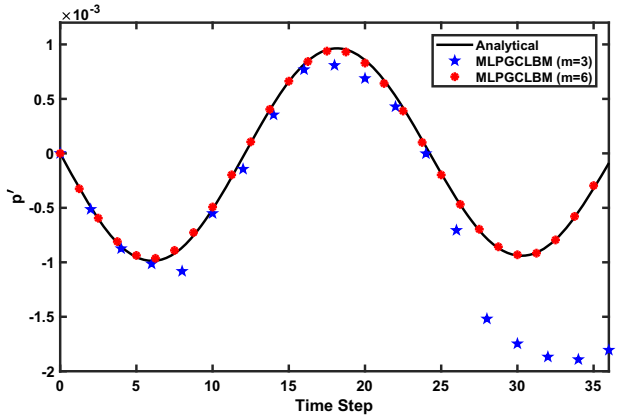

Fig. 6 Acoustic pressure $[\frac{kg}{\Delta x \Delta t^2}]$ versus time step $[\Delta t]$ for $\nu = 1.0 \times 10^{-2}$ $[\frac{\Delta x^2}{\Delta t}]$ with $N_{\text{ppw}} = 14$ points per wavelength with irregular nodal distributions

Table 2 Parameters for the planar pulse wave

Variables	$p'(x, y, 0)$	ρ'	u'	v'	A	σ
Description	$A \exp\left(-\ln(2)\,\frac{x^2}{\sigma^2}\right)$	$\frac{p'}{c_s^2}$	$\frac{p'}{\rho_0 c_s}$	0	$10^{-3} p_0$	0.06–0.11

delta function in parts of the MLPGC-LBM solver. We observe instead how the results of MLPGC-LBM with quadric basis functions dramatically improve and very closely reproduce the analytical acoustic pressure.

3.2 Planar pulse wave

As a second case, the study of a planar pulse wave is carried out by choosing a planar pulse of Gaussian shape located at the center of the domain. The dissipation and dispersion relations are generated from the spatial analysis of Eq. (26) as follows [51]:

$$c_S = \sqrt{2} c_s \sqrt{\frac{1 + (\omega\tau_s)^2}{\sqrt{1 + (\omega\tau_s)^2} + 1}}, \tag{29.1}$$

$$\alpha_S = \frac{\omega}{\sqrt{2} c_s} \sqrt{\frac{\sqrt{1 + (\omega\tau_s)^2} - 1}{1 + (\omega\tau_s)^2}} \tag{29.2}$$

where $\tau_s = 2\nu/c_s^2$. The planar pulse propagates throughout the domain. The assumptions are shown in Table 2. It should be noted that periodic boundary conditions are imposed.

To study the behavior of meshless local Petrov–Galerkin cumulant lattice Boltzmann method (MLPGC-LBM) in a pulse wave emission, we followed Refs. [5,39]. Thus, different viscosities and resolutions σ are considered. The acoustic pressure time history for $\nu = 1.0 \times 10^{-2}$ $[\frac{\Delta x^2}{\Delta t}]$ with $\sigma = 0.11$ is presented in Fig. 7. It shows the comparison between the cumulant LBM (dashed red line) and the MLPGC-LBM results with linear basis functions ($m = 3$) (blue pentagram) and quadric basis functions ($m = 6$) (solid black line). Data are taken at 0, 5, 11, and 17 nodes apart from the center of the domain showing that the intensity loss at any location is proportional to the propagation distance [5,39,51]. It should be noted that the deviations between the cumulant LBM and MLPGC-LBM with linear or quadric basis functions are minor.

In general, the resolution σ is a parameter which can have an effective impact on the accuracy of LBM results. Figure 8 shows the acoustic pressure time history for $\nu = 1.0 \times 10^{-2}$ $[\frac{\Delta x^2}{\Delta t}]$, with $\sigma = 0.06$. It shows that by reducing σ the number of nodes inside the pulse reduces, which produces wiggling in the cumulant LBM results (dashed red line). On the other hand, combinations of LBM and Mfree methods such as local radial point interpolation cumulant lattice Boltzmann method (LRPIC-LBM) (solid black line) and meshless

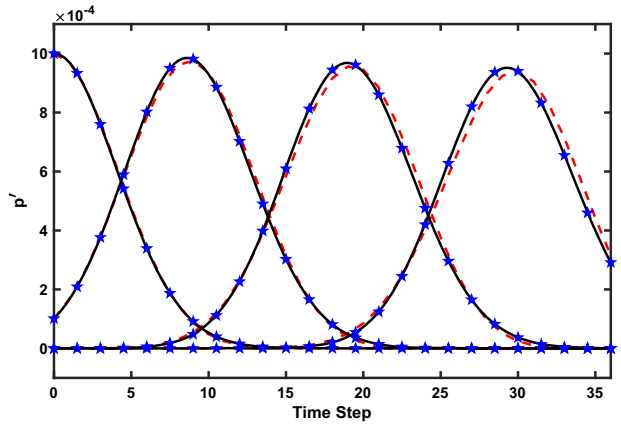

Fig. 7 Acoustic pressure $[\frac{kg}{\Delta x \Delta t^2}]$ versus time step $[\Delta t]$ for $\nu = 1.0 \times 10^{-2}$ $[\frac{\Delta x^2}{\Delta t}]$ with $\sigma = 0.11$: cumulant LBM (dashed red line), MLPGC-LBM (m = 6) (solid black line), and MLPGC-LBM (m=3) (blue pentagram) (color figure online)

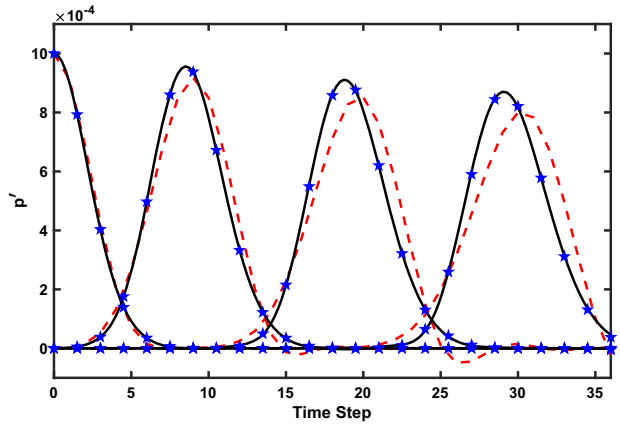

Fig. 8 Acoustic pressure $[\frac{kg}{\Delta x \Delta t^2}]$ versus time step $[\Delta t]$ for $\nu = 1.0 \times 10^{-2}$ $[\frac{\Delta x^2}{\Delta t}]$ with $\sigma = 0.06$: cumulant LBM (dashed red line), LRPIC-LBM (solid black line), and MLPGC-LBM (m=3) (blue pentagram) (color figure online)

local Petrov–Galerkin cumulant lattice Boltzmann method (MLPGC-LBM) with linear basis functions (blue pentagram) behave smoothly. These two Mfree-LB methods give the same results for this setup, but the average run time for MLPGC-LBM is 0.289 times the LRPIC-LBM run time per iteration. The comparison of the ratio $\widehat{p'}(x, \omega) / \widehat{p'}(x, 0)$, as a function of the angular frequency, between LRPIC-LBM and analytical solutions [39] shows that LRPIC-LBM with $\sigma = 0.06$ successfully predicts the theoretical results. And since MLPGC-LBM data closely follow those of LRPIC-LBM, therefore, this method can successfully simulate wave propagation even at small resolutions.

The acoustic pressure time history for $\nu = 1.0 \times 10^{-2}$ $[\frac{\Delta x^2}{\Delta t}]$ with $\sigma = 0.11$ for irregular nodes (Fig. 1b) is depicted in Fig. 9. Cumulant LBM and meshless local Petrov–Galerkin cumulant lattice Boltzmann method (MLPGC-LBM) results with linear basis functions ($m = 3$) and quadric basis functions ($m = 6$) are represented by a dashed red line, blue pentagram with blue line, and a solid black line, respectively. Figure 9 shows that this method with linear basis functions cannot predict wave propagation, which traces back to the lack of a delta function property in the MLPGM scheme. Therefore, as in the temporal analysis of Sect. 3.1, the solution shows instabilities. On the other hand, by using quadric basis functions, one can obtain the same results as with a regular nodal distribution.

3.3 Acoustic pulse

A 2D acoustic pulse is studied as the most standard aeroacoustic 2D benchmark case [52]. This is categorized as a type of circular wave propagation, with a pulse which is considered as Gaussian in shape. The assumptions

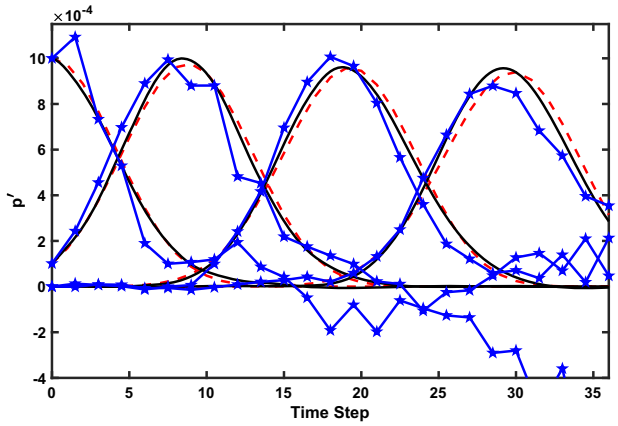

Fig. 9 Acoustic pressure $[\frac{kg}{\Delta x \Delta t^2}]$ versus time step $[\Delta t]$ for $\nu = 1.0 \times 10^{-2}$ $[\frac{\Delta x^2}{\Delta t}]$ with $\sigma = 0.11$: cumulant LBM (dashed red line), MLPGC-LBM (m = 6) (solid black line), and MLPGC-LBM (m=3) (blue pentagram with blue line) (color figure online)

Table 3 Parameters for the 2D acoustic pulse

Variables	ρ'	u'	v'	ϵ	α	σ	r
Description	$\epsilon \exp\left(-\alpha r^2\right)$	0	0	10^{-3}	$\frac{\ln(2)}{\sigma^2}$	$0.11 - 0.04$	$\sqrt{x^2 + y^2}$

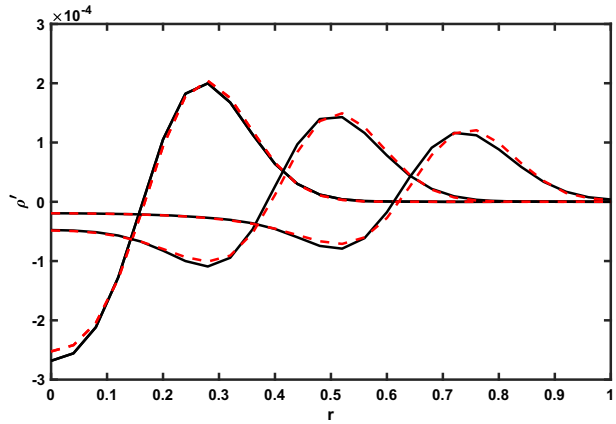

Fig. 10 Propagation of the density perturbation through the domain for $\nu = 1.0 \times 10^{-2}$ $[\frac{\Delta x^2}{\Delta t}]$ with $\sigma = 0.11$ for time steps 10, 20 and 30 from left to right.: Cumulant LBM (solid black line), MLPGC-LBM (m=6) (dashed red line) (color figure online)

of the setup are written in Table 3. Even though periodic boundary conditions are chosen, the total simulation time is limited so as to prevent any boundary effects. In this study, an acoustic pulse generated by an initial Gaussian pressure distribution expands from the center of the domain.

Figure 10 draws a comparison between the solutions of the cumulant LBM (solid black line) and the meshless local Petrov–Galerkin cumulant LBM with quadric basis functions ($m = 6$) (dashed red line). The plot represents the density perturbation obtained with the parameters $\nu = 1.0 \times 10^{-2}$ $[\frac{\Delta x^2}{\Delta t}]$ and $\sigma = 0.11$ as a function of the radial distance for three time steps: 10, 20, and 30. There is a good agreement between both methods when σ is equal to 0.11 or larger, and the deviations are small.

In the study of the propagation of the circular acoustic pulse, the parameter σ can also affect the accuracy of the LBM results. This is shown in Fig. 11, which represents the density function of the acoustic pulse propagation for $\nu = 1.0 \times 10^{-2}$ $[\frac{\Delta x^2}{\Delta t}]$ with $\sigma = 0.04$ for time steps 10, 20, and 30. Here, the same behavior as in planar acoustic waves is found: by reducing σ, the number of nodes inside the pulse is also reduced, which causes the wiggling seen in the cumulant LBM density wave. Figure 11 shows that the cumulant LBM is less stable at low resolutions.

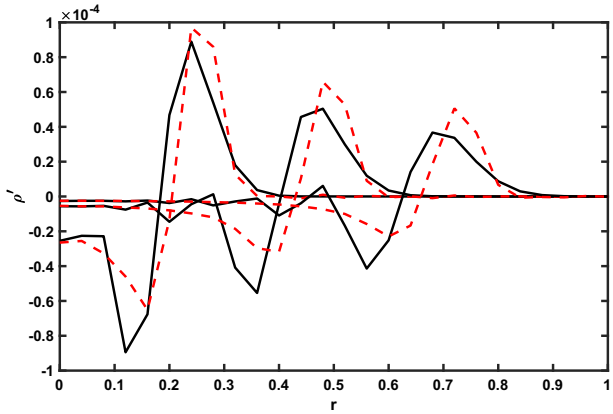

Fig. 11 Propagation of the density perturbation through the domain for $\nu = 1.0 \times 10^{-2}$ $[\frac{\Delta x^2}{\Delta t}]$ with $\sigma = 0.04$ for time steps 10, 20, and 30 from left to right. Cumulant LBM (solid black line), MLPGC-LBM ($m = 6$) (dashed red line) (color figure online)

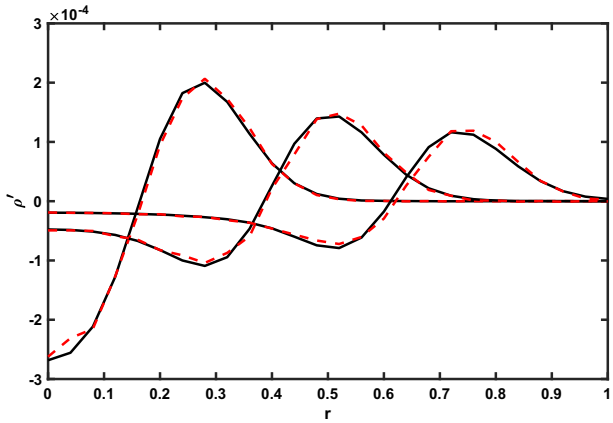

Fig. 12 Propagation of the density perturbation through the irregular nodal distribution for $\nu = 1.0 \times 10^{-2}$ $[\frac{\Delta x^2}{\Delta t}]$ with $\sigma = 0.11$ for time steps 10, 20, and 30 from left to right.: Cumulant LBM (solid black line), MLPGC-LBM (m=6) (dashed red line) (color figure online)

Table 4 Parameters for the acoustic point source

Variables	ρ'	ω	B	r	T
Description	$B\sin(\omega t)$	$\frac{2\pi}{T}$	10^{-2}	$\sqrt{x^2+y^2}$	10–20

The propagation of the circular acoustic pulse for $\nu = 1.0\times10^{-2}$ $[\frac{\Delta x^2}{\Delta t}]$ with $\sigma = 0.11$ for an irregular nodal distribution and time steps 10, 20, and 30 (Fig. 1b) is illustrated in Fig. 12. The results of the meshless local Petrov–Galerkin cumulant LBM with quadric basis functions ($m = 6$) and the cumulant LBM are represented by a dashed red line and a solid black line, respectively. Figure 12 shows that this method, using quadric basis functions, can predict the same results as with regular nodes.

3.4 Acoustic point source

In this Section, to further demonstrate the abilities of the meshless local Petrov–Galerkin cumulant LBM in simulating 2D problems, another test case will be studied: the infinite waves generated by a point source which transmits a sinusoidal signal. The assumptions for this setup are listed in Table 4. To model this point source, a sinusoidal density function is set up at the center node of the domain as in Refs. [5], and periodic boundary conditions are used.

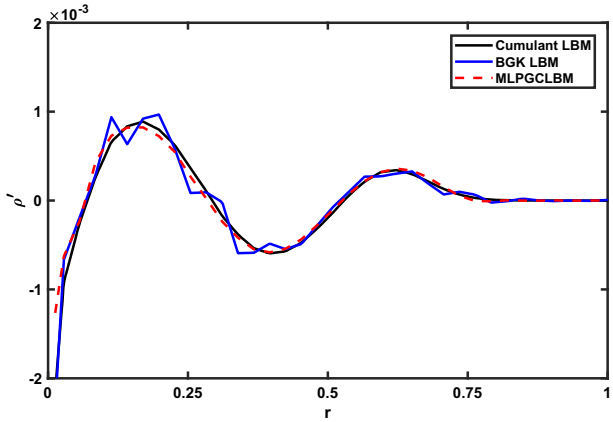

Fig. 13 Comparison of the values of the density perturbation with a period $T = 20\ [\Delta t]$

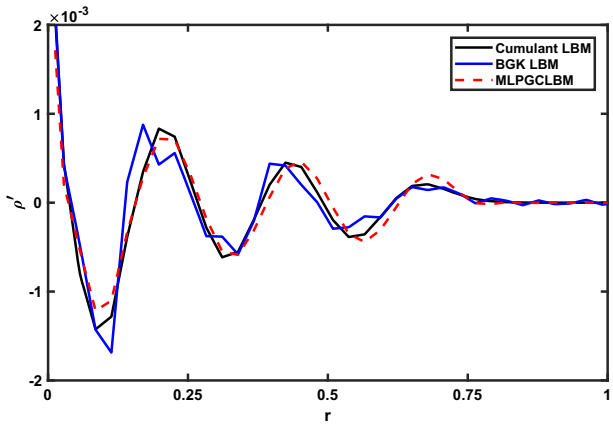

Fig. 14 Comparison of the values of the density perturbation with a period $T = 10\ [\Delta t]$

The propagation of the density function of the acoustic point source wave for $\nu = 1.0 \times 10^{-2}\ [\frac{\Delta x^2}{\Delta t}]$ with a period $T = 20[\Delta t]$ is shown in Fig. 13. The meshless local Petrov–Galerkin cumulant (MLPGC-LBM) result is drawn with a dashed red line while the standard cumulant, and standard BGK LBM results are shown with a solid black line and a solid blue line, respectively. MLPGC-LBM shows a good agreement with the cumulant LBM at a relatively suitable period $T = 20[\Delta t]$. The BGK LBM result follows the other curves, but it displays noisy behavior, as the method is here unstable.

The period T, like σ, is a parameter which can have effects on the accuracy of LBM results. Figure 14 presents the propagation of the density function of the acoustic point source wave for $\nu = 1.0 \times 10^{-2}\ [\frac{\Delta x^2}{\Delta t}]$, with periods $T = 10$. It illustrates that by reducing the period, the number of nodes inside the waves is reduced, which yields worse results for the BGK LBM (solid blue line) than the previous simulation. In fact, the deviation between the cumulant (solid black line) and the meshless local Petrov–Galerkin cumulant LBM (dashed red line) increases for $T = 10$.

A similar analysis can be performed on the same problem using an irregular nodal distribution for the methods under consideration, with analogous results. As an example, the propagation of the density function of the acoustic point source wave for $\nu = 1.0 \times 10^{-2}\ [\frac{\Delta x^2}{\Delta t}]$ with period $T = 20[\Delta t]$ for an irregular nodal distribution is depicted in Fig. 15. It shows small deviations between the meshless local Petrov–Galerkin cumulant (MLPGC-LBM) (dashed red line) and the cumulant LBM (solid black line).

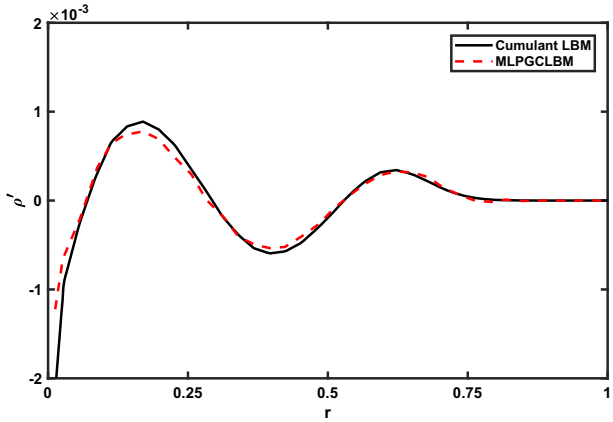

Fig. 15 Comparison of the values of the density perturbation with a period $T = 20\ [\Delta t]$ propagating through an irregular nodal distribution

4 Conclusions

In this paper, propagation of point and planar acoustic waves comprising the temporal decay of a standing plane wave, the spatial decay of a planar acoustic pulse, and the propagation of circular waves, in most real cases, are modeled by the meshless local Petrov–Galerkin cumulant lattice Boltzmann method (MLPGC-LBM). In this model, the collision step is modeled by the cumulant method, and the streaming step is discretized first in time based on the Lax–Wendroff scheme, then in space according to the meshless local Petrov–Galerkin method, a mesh-free method (MLPG). The comparison drawn between the results of MLPGC-LBM and LRPIC-LBM, cumulant LBM, and the analytical solution, illustrates that the acoustic pressure time history for LB methods has a similar behavior, and the errors of the phase speed and the dissipation rate at high enough N_{ppw} and σ are negligible. Moreover, the decrease of the viscosity does not undermine the stability of these two LB methods due to the advantages of the cumulant method. However, the meshless local Petrov–Galerkin cumulant lattice Boltzmann method predicts the same acoustic pressure time history as the local radial point interpolation cumulant lattice Boltzmann method but with shorter run times, and the error of both the phase speed and the dissipation rate for low N_{ppw} and σ are negligible thanks to the properties of the Mfree method. Furthermore, using MLPGC-LBM with irregular nodal distributions and linear basis functions to simulate the propagation of acoustic waves does not give correct results; thus, quadric basis functions are needed due to inaccuracies generated by the lack of delta function properties in the MLPGM scheme. Moreover, simulating circular propagations (acoustic 2D pulse and acoustic point source) show that when the number of points per wavelength is high, the deviations between the MLPGC-LBM and cumulant LBM are low and vice versa, reproducing the same results as planar acoustic wave. To conclude, the possibility of scattering the computational nodes through the domain depending on problem conditions (such as geometries), the accuracy achieved by MLPG, and the high stability provided by the cumulant LBM, make MLPG-LBM a good alternative to conventional methods to model complex engineering problems, especially in aeroacoustics.

Acknowledgements This work has been funded by the Spanish Ministry of Economy, Industry and Competitiveness Research National Agency (under project DPI2016-75791-C2-1-P), by FEDER funds and by Generalitat de Catalunya—AGAUR (under project 2017 SGR 01234), ministerio de economía, industria y competitividad, gobierno de españa (BES-2018-080566).

Declarations

Data availability Authors can confirm that all relevant data are included in the article.

Conflict of interest The authors declare that they have no conflict of interest.

References

1. Kian Far, E., Geier, M., Kutscher, K., Krafczyk, M.: Implicit large eddy simulation of flow in a micro-orifice with the cumulant lattice boltzmann method. Computation (2017). https://doi.org/10.3390/computation5020023

2. Javadi, K., Kazemi, K.: Microgravity modulation effects on free convection problems lbm simulation. Phys. Fluids **30**(1), 017104 (2018)
3. Fard, E.G.: A cumulant lbm approach for large eddy simulation of dispersion microsystems. PhD thesis, Univ.-Bibl (2015)
4. Filippova, O., Hänel, D.: Grid refinement for lattice-bgk models. J. Comput. Phys. **147**(1), 219–228 (1998). https://doi.org/10.1006/jcph.1998.6089
5. Gorakifard, M., Cuesta, I., Salueña, C., Far, E.K.: Acoustic wave propagation and its application to fluid structure interaction using the cumulant lattice Boltzmann method. Comput. Math. Appl. **87**, 91–106 (2021)
6. He, X., Luo, L.S., Dembo, M.: Some progress in lattice Boltzmann method. Part i. Nonuniform mesh grids. J. Comput. Phys. **129**(2), 357–363 (1996). https://doi.org/10.1006/jcph.1996.0255
7. He, X., Doolen, G.: Lattice Boltzmann method on curvilinear coordinates system: flow around a circular cylinder. J. Comput. Phys. **134**(2), 306–315 (1997). https://doi.org/10.1006/jcph.1997.5709
8. Mei, R., Shyy, W.: On the finite difference-based lattice Boltzmann method in curvilinear coordinates. J. Comput. Phys. **143**(2), 426–448 (1998)
9. Xi, H., Peng, G., Chou, S.H.: Finite-volume lattice Boltzmann method. Phys. Rev. E **59**(5), 6202 (1999)
10. Nannelli, F., Succi, S.: The lattice Boltzmann equation on irregular lattices. J. Stat. Phys. **68**(3–4), 401–407 (1992)
11. Peng, G., Xi, H., Duncan, C., Chou, S.H.: Finite volume scheme for the lattice Boltzmann method on unstructured meshes. Phys. Rev. E **59**(4), 4675 (1999)
12. Lee, T., Lin, C.L.: A characteristic Galerkin method for discrete Boltzmann equation. J. Comput. Phys. **171**(1), 336–356 (2001). https://doi.org/10.1006/jcph.2001.6791
13. Li, Y., LeBoeuf, E.J., Basu, P.K.: Least-squares finite-element scheme for the lattice Boltzmann method on an unstructured mesh. Phys. Rev. E **72**, 046711 (2005). https://doi.org/10.1103/PhysRevE.72.046711
14. Min, M., Lee, T.: A spectral-element discontinuous Galerkin lattice Boltzmann method for nearly incompressible flows. J. Comput. Phys. **230**(1), 245–259 (2011). https://doi.org/10.1016/j.jcp.2010.09.024
15. Shu, C., Niu, X., Chew, Y.: Taylor-series expansion and least-squares-based lattice Boltzmann method: two-dimensional formulation and its applications. Phys. Rev. E **65**(3), 036708 (2002)
16. Shu, C., Chew, Y., Niu, X.: Least-squares-based lattice Boltzmann method: a meshless approach for simulation of flows with complex geometry. Phys. Rev. E **64**(4), 045701 (2001)
17. Fard, E.G., Shirani, E., Geller, S.: The fluid structure interaction with using of lattice Boltzmann method. In: 13th Annual International Conference Fluid Dynamic Conference, Shiraz, Iran (2010)
18. Liu, G.R., Gu, Y.T.: An Introduction to Meshfree Methods and their Programming. Springer Science & Business Media, Dordrecht, The Netherlands (2005)
19. Liu, G.R.: Meshfree Methods: Moving Beyond the Finite Element Method. CRC Press, Boca Raton, Florida, USA (2009)
20. Slater, J.C.: Electronic energy bands in metals. Phys. Rev. **45**(11), 794 (1934)
21. Frazer, R.A., Jones, W.N.P., Skan, S.W.: Approximations to Functions and to the Solutions of Differential Equations. HSMO, London (1937)
22. Chorin, A.J.: Numerical study of slightly viscous flow. J. Fluid Mech. **57**(4), 785–796 (1973)
23. Girault, V.: Theory of a finite difference method on irregular networks. SIAM J. Numer. Anal. **11**(2), 260–282 (1974)
24. Perrone, N., Kao, R.: A general finite difference method for arbitrary meshes. Comput. Struct. **5**(1), 45–57 (1975)
25. Snell, C., Vesey, D., Mullord, P.: The application of a general finite difference method to some boundary value problems. Comput. Struct. **13**(4), 547–552 (1981)
26. Gingold, R.A., Monaghan, J.J.: Smoothed particle hydrodynamics: theory and application to non-spherical stars. Mon. Not. R. Astron. Soc. **181**(3), 375–389 (1977)
27. Monaghan, J.J., Lattanzio, J.C.: A refined particle method for astrophysical problems. Astron. Astrophys. **149**, 135–143 (1985)
28. Nayroles, B., Touzot, G., Villon, P.: Generalizing the finite element method: diffuse approximation and diffuse elements. Comput. Mech. **10**(5), 307–318 (1992)
29. Liu, G., Gu, Y.: A local radial point interpolation method (lrpim) for free vibration analyses of 2-d solids. J. Sound Vib. **246**(1), 29–46 (2001)
30. Liu, G., Gu, Y.: A local point interpolation method for stress analysis of two-dimensional solids. Struct. Eng. Mech. **11**(2), 221–236 (2001)
31. Atluri, S.N., Zhu, T.: A new meshless local Petrov-Galerkin (mlpg) approach in computational mechanics. Comput. Mech. **22**(2), 117–127 (1998)
32. Musavi, S.H., Ashrafizaadeh, M.: Meshless lattice Boltzmann method for the simulation of fluid flows. Phys. Rev. E **91**(2), 023310 (2015)
33. Musavi, S.H., Ashrafizaadeh, M.: Development of a three dimensional meshless numerical method for the solution of the Boltzmann equation on complex geometries. Comput. Fluids **181**, 236–247 (2019)
34. Tanwar, S.: A meshfree-based lattice boltzmann approach for simulation of fluid flows within complex geometries: application of meshfree methods for lbm simulations. In: Analysis and Applications of Lattice Boltzmann Simulations, 1st edn, pp. 188–222. IGI Global, USA (2018). https://doi.org/10.4018/978-1-5225-4760-0.ch006
35. Kian Far, E., Geier, M., Krafczyk, M.: Simulation of rotating objects in fluids with the cumulant lattice Boltzmann model on sliding meshes. Comput. Math. Appl. (2018). https://doi.org/10.1016/j.camwa.2018.08.055
36. Pribec, I., Becker, T., Fattahi, E.: A strong-form off-lattice Boltzmann method for irregular point clouds. Symmetry **13**(10), 1802 (2021)
37. Kian Far, E., Geier, M., Kutscher, K., Konstantin, M.: Simulation of micro aggregate breakage in turbulent flows by the cumulant lattice Boltzmann method. Comput. Fluids **140**, 222–231 (2016). https://doi.org/10.1016/j.compfluid.2016.10.001
38. Kian Far, E., Langer, S.: Analysis of the cumulant lattice Boltzmann method for acoustics problems. In: The 13th International Conference on Theoretical and Computational Acoustics, Vienna, Austria (2017)
39. Gorakifard, M., Salueña, C., Cuesta, I., Far, E.K.: Analysis of aeroacoustic properties of the local radial point interpolation cumulant lattice Boltzmann method. Energies (2021). https://doi.org/10.3390/en14051443

40. Seeger, S., Hoffmann, H.: The cumulant method for computational kinetic theory. Contin. Mech. Thermodyn. **12**(6), 403–421 (2000)
41. Seeger, S., Hoffmann, K.: The cumulant method for the space-homogeneous Boltzmann equation. Contin. Mech. Thermodyn. **17**(1), 51–60 (2005)
42. Geier, M. et al.: Ab initio derivation of the cascaded lattice Boltzmann automaton. University of Freiburg–IMTEK (2006)
43. Gorakifard, M., Salueña, C., Cuesta, I., Kian Far, E.: Acoustical analysis of fluid structure interaction using the cumulant lattice Boltzmann method. In: The 16th International Conference for Mesoscopic Methods in Engineering and Science, Heriot-Watt University, Edinburgh, Scotland (2019)
44. Far, K., Geier, M., Krafczyk, M.: A sliding mesh lbm approach for the simulation of the rotating objects. In: Proceedings of the 13th International Conference for Mesoscopic Methods in Engineering and Science, Hamburg, Germany, vol. 22 (2016)
45. Kian Far, E., Geier, M., Kutscher, K., Krafczyk, M.: Distributed cumulant lattice Boltzmann simulation of the dispersion process of ceramic agglomerates. J. Comput. Methods Sci. Eng. **16**(2), 231–252 (2016)
46. Geier, M., Schönherr, M., Pasquali, A., Krafczyk, M.: The cumulant lattice Boltzmann equation in three dimensions: theory and validation. Comput. Math. Appl. **70**(4), 507–547 (2015)
47. Kian Far, E., Gorakifard, M., Fattahi, E.: Multiphase phase-field lattice Boltzmann method for simulation of soluble surfactants. Symmetry (2021). https://doi.org/10.3390/sym13061019
48. Far, K.: Turbulent flow simulation of dispersion microsystem with cumulant lattice Boltzmann method. In: Proceedings of the Formula X, Manchester, UK 24 (2019)
49. Lancaster, P., Salkauskas, K.: Surfaces generated by moving least squares methods. Math. Comp. **37**(155), 141–158 (1981)
50. Kinsler, L.E., Frey, A.R., Coppens, A., Sanders, J.: Fundamentals of acoustics. Amer. J. Phys. **19**(4), 254–255 (1951)
51. Bres, G., Pérot, F., Freed, D.: Properties of the lattice Boltzmann method for acoustics. In: 15th AIAA/CEAS Aeroacoustics Conference (30th AIAA Aeroacoustics Conference), pp. 3395 (2009)
52. Gendre, F., Ricot, D., Fritz, G., Sagaut, P.: Grid refinement for aeroacoustics in the lattice Boltzmann method: a directional splitting approach. Phys. Rev. E **96**(2), 023311 (2017)